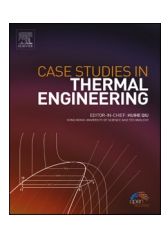


Contents lists available at ScienceDirect

Case Studies in Thermal Engineering

journal homepage: www.elsevier.com/locate/csite



Thermal dynamics of nanofluids with aggregating nanoparticles and magnetic heating: Utilization of Maxwell-Bruggeman and Kreiger-Dougherty models

Muhammad Idrees Afridi a,b,c,*, Abdullah Alhushaybari d, Ali J. Chamkha e

- ^a Research Center for Mathematical Modeling and Simulation, Hanjiang Normal University, Shiyan, 442000, China
- ^b Department of Mathematics, Saveetha School of Engineering, SIMATS, Saveetha University, Chennai 602105, Tamil Nadu, India
- ^c Applied Science Research Center, Applied Science Private University, Amman, 11931, Jordan
- ^d Department of Mathematics, Turabah University College, Taif University, Taif, Saudi Arabia
- e Faculty of Engineering, Kuwait College of Science and Technology, Doha District, 35004, Kuwait

ARTICLE INFO

Keywords: Heat transfer TiO₂/EGnanofluid Maxwell-Bruggeman and Kreiger-Dougherty models Nanoparticles aggregation Entropy generation Local non-similar method (LNSM)

ABSTRACT

Nanoparticle aggregation plays a critical role in enhancing heat transfer processes across various industries. Controlling nanoparticle aggregation can significantly improve thermal efficiency in energy systems, such as solar thermal collectors. Furthermore, in electronic cooling applications, understanding nanoparticle behaviour is vital for optimizing heat dissipation in micro and nanoscale devices. Given the wide-ranging significance of these applications, the current study concentrates on the mathematical modelling and numerical computation of local non-similar flow through a stretching surface coupled with nanoparticle aggregation. Because of viscous dissipation, a constant wall temperature causes local non-similarity, which is a key novelty of our present work. Furthermore, this investigation examines the impact of a uniform magnetic force on heat transfer and fluid flow. The Maxwell-Bruggeman and Kreiger-Dougherty models are used to represent accurately the viscosity and thermal conductivity of a nanofluid containing aggregated nanoparticles. Additionally, the study examines the entropy generation within a local non-similar nanofluid flow featuring nanoparticle aggregation. The pseudo-similarity variable, stream-wise transformed coordinates, dimensionless velocity components, and temperature are used to transform the set of governing equations and associated boundary conditions into dimensionless form. These non-dimensional equations are developed to a second level of truncation. For numerical solutions, a robust numerical scheme called the generalized differential quadrature method is implemented. The findings are visually presented and discussed, encompassing both scenarios with and without aggregation. The study provides a numerical comparison of heat transfer enhancement in tabular format concerning the growing values of nanoparticle volume fraction, considering both the presence and absence of aggregation. Notably, the results reveal that heat transfer enhancement is substantially more pronounced in the presence of aggregation than in its absence. Moreover, the analysis underscores that nanoparticle aggregation leads in higher entropy generation. It is observed that when aggregation is not taken into consideration, the velocity profile is lower when it is. Furthermore, it is found that as the values of the transformed stream-wise coordinate, Hartman number and temperature difference parameter grew, Bejan's number profile diminished.

https://doi.org/10.1016/j.csite.2025.106195

^{*} Corresponding author. Research Center for Mathematical Modeling and Simulation, Hanjiang Normal University, Shiyan, 442000, China. *E-mail address:* afridi@hjnu.edu.cn (M.I. Afridi).

1. Introduction

Heat transfer through fluids widely used in industrial applications, including but not limited to water, biofluids, engine oil, ethylene glycol, and lubricants, exhibits low thermal conductivity, leading to inadequate heat transfer capabilities. In comparison, solid metallic substances such as iron, copper, and silver, along with non-metallic materials like copper oxide, silicon carbide, alumina, and carbon nanotubes, exhibit significantly greater thermal conductivities. Low-performing fluids are utilized in various fields, including power generation, manufacturing, transportation, and microelectronics, to facilitate heat transfer. However, their inefficiency reduces thermal transfer from the surface of the fluid. In addressing this issue, nanofluids have been employed as carrier fluids, consisting of a combination of nanoparticles depressed within a base fluid that exhibits greater thermal conductivity. Nanoparticles are characterized by their diminutive dimensions and wide specific surface areas. Because of this, as compared to conventional fluids, nanofluids show remarkable thermophysical properties, for example, high thermal conductivity and convective heat transfer coefficient. The terminology "nanofluid," coined by Choi [1], refers to a colloidal suspension of nanoparticles that are individually smaller than 100 nm and are disseminated inside base fluids (water, lubricants and oils, polymeric solutions and biological fluids). These nanoparticles (NPs) can come in a variety of forms, including oxides such as alumina, copper oxide, and titania; metallic alternatives like silver, copper, and gold; non-metallic substances; graphite, carbon nanotubes, graphene, and graphene oxide; and carbon-based compounds. A wide range of prospective opportunities in several sectors, engineering disciplines, and biology are made possible by nanofluids. Individuals may refer to the extensive research conducted to attain a comprehensive understanding of these applications [2–10].

Numerous physical processes have an impact on the existence of nanoparticles (NPs) in a working fluid. Das et al. [11] investigated the impact of three different kinds of nanoparticles (aluminium oxide, titanium dioxide and copper oxide) on a flow of an electrically conducting nanofluid through a curved stretching sheet. Sarkar et al. [12] investigated the flow of Sisko nanofluid over an elastic stretched cylinder, incorporating the influences of velocity slip, thermal radiation and chemical reactions. Singh et al. [13] analysed the hydromagnetic flow of the nanofluid Ti6Al4V-H₂O over a Darcy-Brinkman porous media embedded in a channel. Hussain et al. [14] conducted various physical quantities of interest in the flow of a kerosene oil-based hybrid nanofluid. Hussain et al. [15] reported several solutions for the buoyancy impacts in the flow of non-Newtonian Cross nanofluids (water + TiO2) through a Darcy-Forchheimer porous media over a vertical surface, considering the experimental properties of the nanofluid and incorporating entropy production along with an irregular heat sink/source. Parvin et al. [16] examined the 2D flow of a Maxwell nanofluid over an inclined shrinking sheet with an exponential shrinking velocity. Heat transfer, along with mass transfer analyses, are performed, considering the Soret and Dufour effects, along with exponential surface temperature and concentration. Mohanty et al. [17] analysed the thermosolutal Marangoni convection in the magnetohydrodynamics stagnation point flow of a hybrid nanofluid (GO–MoS2/water) with the influence of an inclined magnetic field. The stagnation point flow of ternary nanofluid across a porous material was examined

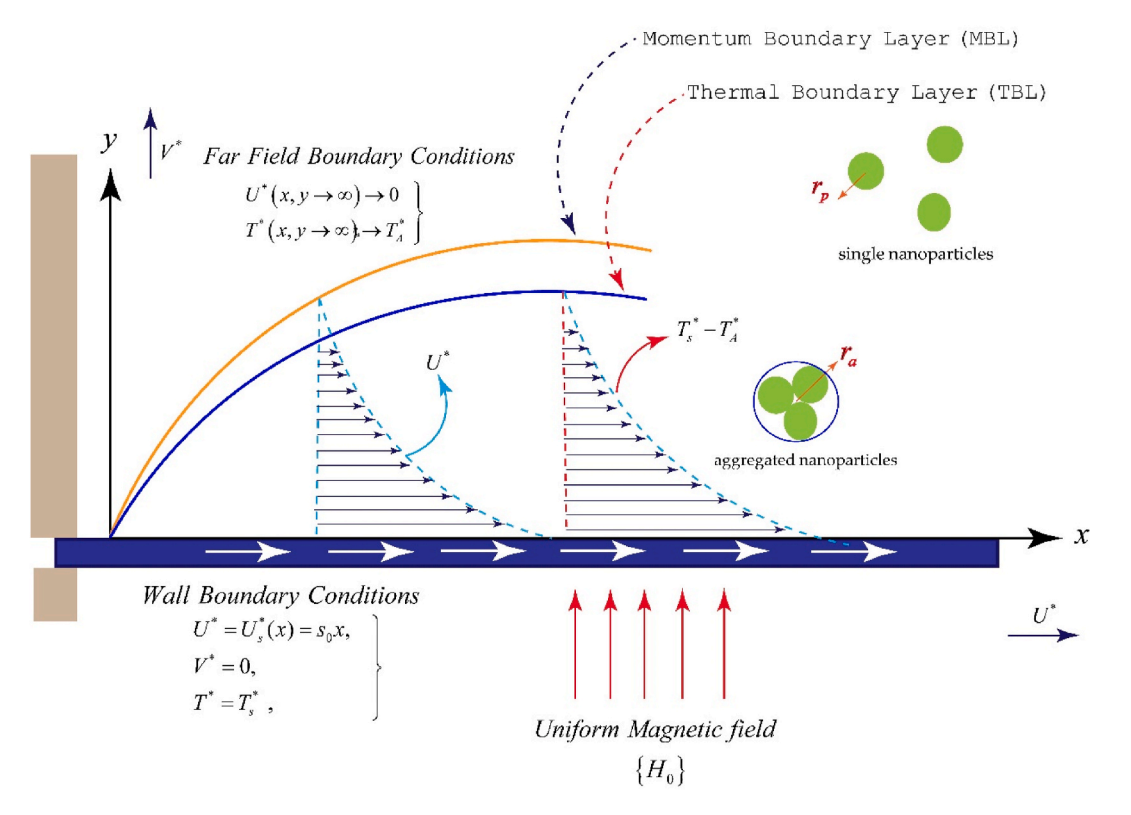


Fig. 1. Geometrical representation.

by Samantaray et al. [18] by incorporating the impacts of radiation and chemical reactions. Their study focuses on how thermal radiation influences heat transfer and how chemical reactions influence the fluid flow and concentration distribution within porous media. Mohanty et al. [19] made an irreversibility analysis of the three-dimensional flow of a non-Newtonian hybrid nanofluid between two rotating disks. Their investigation incorporated Joule dissipation along with nonlinear thermal radiation within the energy equation.

The aggregation of NPs is a fundamental component of the suspension. The primary reason for NP aggregation is the strong covalent and metallic connections between nanoparticles (NPs) [20,21]. The NPs are joined by these covalent and metallic connections to form clusters known as NP aggregates. As a result, NPs are discovered in clustered forms rather than as solitary entities in a base fluid (BF) (see Fig. 1). Using aggregation models to TiO_2/EG nanofluid, Chen et al. [20] found excellent agreement with experimental outcomes. It is found that the traditional model inaccurately predicts the thermophysical properties of nanofluid. As a result, the model

was changed to include the aggregation of nanoparticles. A modified "Krieger-Dougherty model"
$$\left(\frac{\mu_{nf}}{\mu_f} = \left(1 - \frac{\Phi_a}{\Phi_m}\right)^{-[\varepsilon]} \Phi_m\right)$$
 that con-

siders nanoparticle aggregation provides a more realistic estimate of the viscosity of nanofluids (ethylene glycol + titania). It has been conclusively determined that the Maxwell model, as delineated in Table 1, is inappropriate for the estimation of thermal conductivity in titania nanofluids utilizing ethylene glycol as a working fluid. As a result, the Maxwell model was modified $\begin{pmatrix} (k_1+2k_2) & 2\Phi_1(k_1-k_2) \end{pmatrix}$

$$\left(k_{nf} = k_f \left\{\frac{(k_a + 2k_f) + 2\Phi_a(k_a - k_f)}{(k_a + 2k_f) - \Phi_a(k_a - k_f)}\right\}\right) \text{ to include the aggregation of nanoparticles. The structure and aggregation (S&A) of nanoparticles}$$

(NPs) were the primary focus of Motlagh and Kalteh's [22] investigation into heat transport in a specific type of nanochannel. Swain and Mahanthesh [23] investigated the influence of NP AGN and Joule heating on the flow characteristics of nanomaterials. Sabu et al. [24] reported the dynamics of nanoparticles in an AGN stream flowing through a convective nanofluid on an inclined flat surface. Mahanthesh [25] conducted a study on heat transport in nanoliquid flow, with a specific focus on the phenomenon of NP (Nanoparticle) aggregation. Additionally, a study conducted by Mackolil and Mahanthesh [26] aimed to scrutinise the influence of the Lorentz force on nanofluid by investigating the aggregation behaviour of NPs.

Boundary layer flow and transport phenomena over a different surfaces have numerous practical applications, including but not limited to polymer processing technology, polymer sheet extrusion, cooling of filaments, continuous casting, and aerodynamics extrusion [27-36] Researchers have endeavoured to elucidate the correlation between the dependent and independent variables within the governing equations pertaining to boundary layer flow in order to investigate the boundary layer phenomena driven by stretching sheets. The process of this transformation involves the reduction of multiple independent variables into a single independent variable, leading to the development of self-similar equations. The derivation of self-similar boundary layer equations, while considering the impact of viscous dissipation, can present considerable challenges. The occurrence of frictional heating is inevitable because of the substantial velocity gradients within the boundary layer regions. To obtain self-similar solutions under the influence of frictional dissipation, researchers often impose certain limitations on the thermal boundary condition by selecting a distinctive variable boundary temperature to identify suitable similarity variables. The application of transformations to the energy equation may result in the emergence of a constraint. The self-similar behaviour of the equations governing the flow induced by a linearly stretched sheet $u_s(x) = s_0 x$ is contingent upon the presence of a non-uniform boundary temperature distribution, i.e. the temperature profile of the stretching boundary should be parabolic $T_s(x) = T_A + T_r x^2$ [37,38]. The research carried out by Cortell [39] scrutinized the flow characteristics through a non-linearly stretching sheet with a specific velocity profile $u_s(x) = s_0 x^n$ and wall temperature $T_s(x) = T_A + t$ $T_r x^p$, with particular emphasis on the impact of frictional dissipation. The possibility of a self-similar solution was observed in cases where p = 2n. Afridi et al. [40] conducted a study that placed its primary focus on analysing the entropy production associated with a flow past over a non-flat porous stretched surface subjected to a specific temperature constraint on the surface $T_s(x) = T_A + T_A$ $T_r(x+b)^{(1-n)/2}$ and the velocity $u_s(x)=u_0(x+b)^m$. A similarity solution in presence of viscous dissipation has been identified to exist when n = 1 - 4m. Megahed [41] conducted an examination into the flow characteristics of Williamson fluid over a nonlinearly

Table 1Thermophysical properties in presence and absence of nanoparticle aggregation.

Properties	without aggregation	with aggregation
Thermal conductivity	$k_{nf} = k_f igg\{ rac{(k_p + 2k_f) + 2\Phi(k_p - k_f)}{(k_p + 2k_f) - \Phi(k_p - k_f)} igg\},$	$k_{nf} = k_f iggl\{ rac{\left(k_a + 2k_f ight) + 2\Phi_a\left(k_a - k_f ight)}{\left(k_a + 2k_f ight) - \Phi_a\left(k_a - k_f ight)} iggr\},$
Heat capacitance	$(ho c_p)_{nf} = egin{cases} (1-\Phi)(ho c_p)_f \ +\Phi(ho c_p)_f(ho c_p)_p \end{cases}$	$\left(ho c_p ight)_{nf} = \left\{egin{array}{l} (1-\Phi_a)(ho c_p)_f \ +\Phi_a(ho c_p)_f(ho c_p)_p \end{array} ight.$
Electric conductivity	$rac{\sigma_{nf}}{\sigma_f} = 1 + rac{3(\sigma-1)\Phi}{2+\sigma-(\sigma-1)\Phi}$	$rac{\sigma_{nf}}{\sigma_f} = 1 + rac{3(\sigma-1)\Phi_a}{2+\sigma-(\sigma-1)\Phi_a}$
	here	here
	$\sigma = rac{\sigma_p}{\sigma_f}$	$\sigma = rac{\sigma_p}{\sigma_f}$
Density	$ ho_{nf}=(1-\Phi) ho_f+\Phi ho_p$	$ ho_{nf} = (1-\Phi_a) ho_f + \Phi_a ho_p$
Dynamic viscosity	$\mu_{n\!f} = rac{\mu_f}{(1-\Phi)^{2.5}}$	$rac{\mu_{nf}}{\mu_f} = \left(1 - rac{\Phi\left(rac{r_a}{r_p} ight)^{3-D}}{\Phi_m} ight)^{-\left[arepsilon ight]\Phi_m}$
		,, ()

stretched $(u_s(x) = u_0 x^k)$ and radiative non-isothermal surface $(T_s(x) = T_A + T_r x^p)$ by considering the influence of viscous dissipation. To achieve self-similar equations and eliminate the dependence of the non-Newtonian fluid parameter (Weissenberg number) and Eckert number on the spatial coordinate x, specific constraints were enforced i.e. (k = 1/3, p = 2n). The existence of self-similar equations in presence of mixed convection, originating from an exponentially stretched sheet $(u_s(x) = u_r e^{x/L})$ and subjected to viscous heating, has been empirically confirmed by Partha et al. [42] under the imposition of a particular form of wall temperature $(T_s(x) = T_A + T_0 e^{2x/L})$. The constraints on attaining self-similar solutions through the incorporation of viscous heating were delineated in several recent studies [43–45].

The first law of thermodynamics underpins energy conservation and its application in analysing temperature distributions in fluid flow. While the first law addresses the quantity of energy, it does not account for the quality of energy. In contrast, the second law of thermodynamics emphasizes the irreversibility of real-world processes and the degradation of energy quality. Entropy serves as a key metric for quantifying irreversibility and is vital for assessing entropy generation in flow regions. Entropy production in fluid flow processes degrades the quality of energy. Understanding the factors that contribute to entropy generation and identifying parameters that mitigate it is crucial for preserving energy quality. Bejan [46] is recognised as a pioneering researcher who has extensively investigated the factors contributing to entropy generation within the framework of convective heat transfer phenomena. The generation of entropy in fluid flow processes has been attributed to the interplay between temperature gradient and fluid friction (i.e., velocity gradient). Following Bejan's ground-breaking work, scientists have performed second-law analyses to reduce entropy production during heat transfer and fluid flow. Entropy production in the flow of water and ethylene glycol-based nanofluid containing copper and titanium oxide over a stretching cylinder is scrutinized by Mondal et al. [47]. Mahato et al. [48] discussed how the inclined magnetic field and homogeneous and heterogeneous chemical reactions influence entropy production in the unsteady stagnation point flow of nanofluid through a porous media. Afridi and Qasim [49] conducted a comparative study and analysed entropy generation in a flow of Cu-water and Ag-water nanofluids past over a stretching sheet of variable thickness. Chamkha et al. [50] examined entropy production in natural convective magnetohydrodynamic flow of CuO-H2O nanofluid in a C-shaped cavity. Butt and Ali [51] inspected the impacts of radiation and frictional heating on the flow generated by moving surface. Rashidi and Freidoonimehr [52] investigated the impacts of magnetic fields on entropy production and thermal characteristics, providing insights into the complex relationship between fluid flow, porous media, and MHD effects. Makinde [53] conducted an extensive examination focusing on the phenomenon of entropy generation within a magnetohydrodynamic (MHD) boundary layer flow across a planar interface. An entropy production analysis was conducted by Rashidi et al. [54] for stagnation point flow over a porous medium induced by a porous stretching surface. Das et al. [55] explored the flow past over an elastic surface and entropy production in magnetohydrodynamic and thermal boundary layer flow with Newtonian heating. Hakeem et al. [56] examined radiative MHD slip flow, focusing on how nanofluid properties and non-uniform heat sources influence entropy generation and energy dissipation. Sahoo et al. [57] reported a study on entropy production and mixed convective MHD flow of a dissipative nanofluid under hall effects. Chlaihawi et al. [58] compared entropy production between Newtonian and non-Newtonian hybrid nanofluids in enclosures.

Viscous dissipation, the conversion of mechanical energy into thermal energy due to frictional heating, continually alters the energy in fluid systems. The resulting heat generation can impact fluid dynamics by affecting viscosity. The temperature distribution resulting from internal energy production is crucial in industrial contexts to prevent material degradation. Mathematically, this process involves the product of velocity gradient and viscous momentum flux tensor. Dissipation is most pronounced in regions with significant velocity gradients, including boundary layers, shear layers, turbulent wakes, and lubricant flow in rapidly moving components. Reducing dissipation is crucial for lowering power consumption in aircraft wakes and propulsive jets [59–61].

In the present investigation, the inclusion of viscous dissipation reveals non-similar behaviour in the flow over a stretching thin surface at a uniform temperature. However, it's essential to note that some previous studies have incorrectly treated these non-similar equations as self-similar, resulting in significant inaccuracies. A comprehensive review of the literature on flow over an elastic stretching surface reveals that, to date, no study has explored the flow of a nanofluid with aggregation over a stretching sheet in the presence of both viscous and Joule dissipation. Our current research addresses this gap by investigating the non-similar boundary layer flow of nanofluid, both with and without aggregation, over a linearly stretched sheet maintained at a fixed wall temperature. We specifically aim to understand and address non-similar behaviour. Additionally, our investigation involves an analysis of entropy production, taking into account the impacts of Joule dissipation and frictional heating. To accomplish this, we derive the boundary layer equations using the local non-similarity approach up to the second degree of truncation. Subsequently, we employ the generalized differential quadrature method to solve these equations numerically. To compare the numerical outcomes in the presence and absence of nanoparticle (NP) aggregation, we use the slope linear regression method. Furthermore, we explore heat transfer enhancement numerically, both with and without NP aggregation.

2. Statement and mathematical formulation

Consider stretching of an elastic stretching sheet in a steady incompressible nanofluid fluid, which leads to the formation of a boundary layer. As illustrated in Fig. 1, a magnetic field of intensity H_0 is applied perpendicular to the surface being stretched. A constant surface temperature is assumed at the stretching sheet surface, which is denoted by T_s^* . In addition, $U^* = U_s^*(x) = s_0 x$ is supposed to be the velocity of a stretching surface. The following governing equations are based on the previously stated assumptions [62]

$$\frac{\partial U^*}{\partial x} + \frac{\partial V^*}{\partial y} = 0, \tag{1}$$

$$U^* \frac{\partial U^*}{\partial x} + V^* \frac{\partial U^*}{\partial y} = \left(\frac{\mu}{\rho}\right)_{nf} \frac{\partial^2 U^*}{\partial y^2} - \left(\frac{\sigma}{\rho}\right)_{nf} H_0^2 U^*, \tag{2}$$

$$U^* \frac{\partial T^*}{\partial x} + V^* \frac{\partial T^*}{\partial y} = \left(\frac{k}{\rho c_p}\right)_{nf} \frac{\partial^2 T^*}{\partial y^2} + \left(\frac{\mu}{\rho c_p}\right)_{nf} \left(\frac{\partial U^*}{\partial y}\right)^2 + \left(\frac{\sigma}{\rho c_p}\right)_{nf} H_0^2 U^{*2}, \tag{3}$$

$$\left\{ \begin{array}{l}
 U^* = U_s^*(x) = s_0 x, \\
 V^* = 0, \\
 T^* = T_s^*,
 \end{array} \right\}_{at \ v=0},$$

$$\left\{ \begin{array}{l}
 a_t \\
 a_t \\
 &_t \\$$

$$\begin{array}{c} \mathsf{U}^*(x,y\!\to\!\infty)\!\to\!0 \\ \mathsf{T}^*(x,y\!\to\!\infty)\!\to\!T_A^* \end{array} \bigg\}.$$

Eq. (1) presents the continuity equation in differential form for fluid with constant density, illustrating that the net flow of fluid into or out of a control volume is zero, thereby confirming the principle of mass conservation. Equation (2) is derived from the application of Newton's second law of motion to a fluid element. The convective acceleration, which describes the spatial variation of the velocity component \widehat{u} and \widehat{v} , is respectively captured by the first and second terms on the left-hand side of Equation (2). On the right-hand side, the first term represents the viscous force, while the final term corresponds to the influence of the applied magnetic field i. e, incorporating the magnetic field H_0 as a body force. Eq. (3), referred to as the energy equation, is formulated based on the principle of energy conservation. The convective components, identified as the initial and subsequent terms on the left-hand side of Equation (3), elucidate the transfer of energy that arises from the macroscopic movement of the fluid along the x and y axes. These terms elucidate the mechanism by which temperature is advected through the fluid as it moves with velocity components U^* and V^* . The first term on the right-hand side of Equation (3) quantifies the rate of heat conduction within the fluid, representing thermal diffusion driven by the temperature gradient in the y direction. The second term on the right-hand side of Equation (3) accounts for the effects of viscous dissipation, and the last term represents the Joule heating

Boundary condition 4(a) represents the no-slip velocity condition, which means that the velocity of the fluid layer attached to the stretched surface is equal to the velocity of the stretching sheet. Condition 4(b) shows that the velocity component along the y-axis is zero at the surface of the stretched sheet. Condition 4(c) indicates that the surface temperature is maintained at a constant level. Conditions 5(a) and 5(b) show that the velocity and temperature asymptotically approach the free stream velocity and ambient temperature, respectively.

Below, we defined the dimensionless variables for the temperature (g), velocity components $\left(\frac{df}{dh}, f\right)$ and normal distance from the surface of an elastic stretched sheet (h)[48]

$$h = y\sqrt{\frac{s_o}{\nu_f}}, \frac{df}{dh} = \frac{U^*}{s_0 x}, f(h) = -\frac{V^*}{\sqrt{s_0 \nu_f}}, g(h) = \frac{T^* - T_A^*}{T_*^* - T_*^*}.$$
 (6)

Utilizing the relations of (6) in (2)–(5), we get

$$\left(\frac{\Delta_1}{\Delta_2}\right)\frac{d^3f}{dh^3} + f\frac{d^2f}{dh^2} - \left(\frac{df}{dh}\right)^2 - \left(\frac{\Delta_3}{\Delta_2}\right)H_m^2\frac{df}{dh} = 0,\tag{7}$$

$$\left(\frac{\Delta_4}{\Delta_5}\right)\frac{d^2g}{dh^2} + \left(\frac{\Delta_1}{\Delta_5}\right)Ec(x)\Pr\left(\frac{d^2f}{dh^2}\right)^2 + \left(\frac{\Delta_3}{\Delta_5}\right)Ec(x)H_m^2\Pr\left(\frac{df}{dh}\right)^2 + \Pr f(h)\frac{dg}{dh} = 0,$$
(8)

$$\begin{pmatrix} \frac{f(0)}{df(0)} \\ \frac{df(0)}{dh} \\ g(0) \end{pmatrix} = \begin{pmatrix} 0 \\ 1 \\ 1 \end{pmatrix}, \tag{9}$$

$$\begin{pmatrix} \frac{\mathrm{df}(h \to \infty)}{dh} \\ g(h \to \infty) \end{pmatrix} = \begin{pmatrix} 0 \\ 0 \end{pmatrix}.$$
(10)

Due to the dependency between the viscous dissipation parameter Ec(x) and the spatial variable x, the problem is not self-similar, and the transformations in (6) are not applicable. Below is a definition of the space-dependent Eckert number

$$Ec(\mathbf{x}) = \frac{U_s^{*2}}{(c_p)_f(T_s^* - T_A^*)} = \frac{s_0^2 \mathbf{x}^2}{(c_p)_f(T_s^* - T_A^*)}.$$
 (11)

As a result, the basic quantities also vary stream-wise. It is, therefore, necessary to define the transformed stream-wise coordinate $\bar{\xi}(x)$ to convert the governing equations into the local non-similar partial differential equations. It can be accomplished by choosing the local non-similarity variable (transformed stream-wise coordinate) that corresponds to the Eckert number, as given below

$$\overline{\xi}(x) = \frac{s_0 x}{\sqrt{(c_p)_f (T_s^* - T_A^*)}} = \sqrt{Ec(x)}.$$
(12)

Now, introducing stream-wise transformed coordinate and modifying the relations in (6), we have

$$h = y\sqrt{\frac{s_0}{\nu_f}}, \overline{\xi} = \frac{s_0 x}{\sqrt{(c_p)_f}(T_s^* - T_A^*)}, \frac{\partial f(h, \overline{\xi})}{\partial h} = \frac{\overline{U}}{s_0 x},$$

$$f(h, \overline{\xi}) = -\left[\frac{V^*}{\sqrt{s_0 \nu_f}} + \overline{\xi} \frac{\partial f(h, \overline{\xi})}{\partial \overline{\xi}}\right], g(h, \overline{\xi}) = \frac{T^* - T_A^*}{T_s^* - T_A^*}.$$
(13)

Utilizing the relations of (13) in (2)–(5), we get

$$\left(\frac{\Delta_1}{\Delta_2}\right)\frac{\partial^3 f}{\partial h^3} + f\frac{\partial^2 f}{\partial h^2} - \left(\frac{\partial f}{\partial h}\right)^2 - \left(\frac{\Delta_3}{\Delta_2}\right)H_m^2\frac{\partial f}{\partial h} = \xi\left(\frac{\partial f}{\partial h}\frac{\partial^2 f}{\partial h\partial \xi} - \frac{\partial^2 f}{\partial h^2}\frac{\partial f}{\partial \xi}\right),\tag{14}$$

$$\left(\frac{\Delta_{4}}{\Delta_{5}}\right)\frac{\partial^{2}g}{\partial h^{2}} + \left(\frac{\Delta_{1}}{\Delta_{5}}\right)\overline{\xi}^{2} \operatorname{Pr}\left(\frac{\partial^{2}f}{\partial h^{2}}\right)^{2} + \left(\frac{\Delta_{3}}{\Delta_{5}}\right)\operatorname{Pr}H_{m}^{2}\overline{\xi}^{2}\left(\frac{\partial f}{\partial h}\right)^{2} + \operatorname{Pr}f\frac{\partial g}{\partial h} = \begin{cases} \overline{\xi} \operatorname{Pr}\left(\frac{\partial g}{\partial \overline{\xi}}\frac{\partial f}{\partial h} - \frac{\partial g}{\partial h}\frac{\partial f}{\partial \overline{\xi}}\right) \end{cases} \right), \tag{15}$$

$$\begin{pmatrix}
\frac{\partial f(0,\overline{\xi})}{\partial h} \\
f(0,\overline{\xi}) + \overline{\xi} \frac{\partial f(0,\overline{\xi})}{\partial \overline{\xi}} \\
g(0,\overline{\xi})
\end{pmatrix} = \begin{pmatrix} 1 \\ 0 \\ 1 \end{pmatrix},$$
(16)

$$\begin{pmatrix} \frac{\partial f(h \to \infty, \overline{\xi})}{\partial h} \\ g(h \to \infty, \overline{\xi}) \end{pmatrix} = \begin{pmatrix} 0 \\ 0 \end{pmatrix}. \tag{17}$$

The Nusselt number $Nu_x = \frac{xq_s}{k_{bf}(T_s^* - T_A^*)}$ reduces to

$$\frac{Nu_x}{\sqrt{Re_x}} = -\left(\Delta_4\right) \frac{\partial g(0,\overline{\xi})}{\partial h}.\tag{18}$$

Here,

$$\Delta_1 = \frac{\mu_{nf}}{\mu_f}, \Delta_2 = \frac{\rho_{nf}}{\rho_f}, \Delta_3 = \frac{\sigma_{nf}}{\sigma_f},$$

$$\Delta_4 = \frac{k_{nf}}{k_f}, \Delta_5 = \frac{(\rho c_p)_{nf}}{(\rho c_p)_f},$$

$$Pr = \left(\frac{\mu c_p}{k}\right)_f (Prandtl number),$$

$$H_m^2 = \frac{H_0^2 \sigma_f}{s_n \rho_c} (Hartman number).$$

3. Nanofluid thermophysical properties and aggregated nanoparticles

To represent the thermophysical characteristics of nanofluids accurately, it is essential to account for the phenomenon of nanoparticle aggregation. Using aggregation models to TiO_2/EG nanofluid, Chen et al. [20] found excellent agreement with experimental results. A summary of the traditional models that inaccurately predict the thermophysical characteristics of nanofluids and aggregation models is given in Table 1. A modified Krieger-Dougherty model that considers nanoparticle aggregation provides a more realistic

estimate of the viscosity of nanofluids (ethylene glycol + titania). As a result, the relative viscosity can be calculated as follows [20,21]

$$\frac{\mu_{nf}}{\mu_f} = \left(1 - \frac{\Phi_a}{\Phi_m}\right)^{-[\varepsilon] \Phi_m}.\tag{19}$$

Here, Φ_a , Φ_m and $[\epsilon]$ are respectively represent the volume fraction of aggregate, maximum volume fraction and Einstein coefficient. The expression for Φ_a is as follows [20,21]

$$\Phi_a = \Phi\left(\frac{r_a}{r_p}\right)^{3-D}.$$

Here, Φ , r_p and r_a respectively represent nanoparticle volume fraction, radii of nanoparticles and aggregates. Chen et al. [20] reported the suitable values for ethylene glycol-based titania nanofluids as given below

$$\frac{r_{a}}{r_{p}} = 3.34
[\varepsilon] = 2.5
\Phi_{m} = 0.605
D = 1.8$$
(21)

The Maxwell model (Table 1) is inadequate for predicting the thermal conductivity of nanoliquid with Titania nanoparticles suspension. Consequently, the model was modified to incorporate nanoparticle aggregation, as explained below

$$k_{nf} = k_f \left\{ \frac{(k_a + 2k_f) + 2\Phi_a(k_a - k_f)}{(k_a + 2k_f) - \Phi_a(k_a - k_f)} \right\},\tag{22}$$

Here k_a denotes a thermal conductivity of aggregates, and it can be determined by modifying the Bruggeman model as given below [20, 21]

$$k_{a} = 0.25 \begin{bmatrix} (3\Phi_{i} - 1)\frac{k_{p}}{k_{f}} + (3(1 - \Phi_{i}) - 1) \\ + \left\{ \left((3\Phi_{i} - 1)\frac{k_{p}}{k_{f}} + (3(1 - \Phi_{i}) - 1) \right)^{2} + \right\}^{0.5} + 8\frac{k_{p}}{k_{f}} \end{bmatrix}.$$

$$(23)$$

Here,
$$\Phi_i = \left(\frac{r_a}{r_p}\right)^{D-3}$$
.

The Bruggeman and Maxwell models, taken together, improved the accuracy of estimating the effective thermal conductivity of EG-TiO₂ nanoliquids. Table 2 presents the thermal characteristics of the working fluid, Ethylene, and TiO₂ nanoparticles.

4. Local non-similar approach (two-equation model)

Utilizing local non-similar (LNS) methodology, we solve the local non-similar dimensionless governing equations for nanofluids as mentioned in Eqs. (13) and (14) along with the boundary conditions (15)–(17). To obtain the local similarity model from Eqs. (13) and (14), all the derivatives of f and g with respect to the local non-similarity variable are ignored. As a result, the local similarity model or one-equation model is obtained as given below

$$\left(\frac{\Delta_1}{\Delta_2}\right)\frac{\partial^3 f}{\partial h^3} + f\frac{\partial^2 f}{\partial h^2} - \left(\frac{\partial f}{\partial h}\right)^2 - \left(\frac{\Delta_3}{\Delta_2}\right)H_m^2\frac{\partial f}{\partial h} = 0,\tag{24}$$

$$\left(\frac{\Delta_4}{\Delta_5}\right)\frac{\partial^2 \mathbf{g}}{\partial h^2} + \left(\frac{\Delta_1}{\Delta_5}\right) \Pr\left(\frac{\partial^2 f}{\partial h^2}\right)^2 + \left(\frac{\Delta_3}{\Delta_5}\right) \Pr\left(\frac{\partial f}{\partial h}\right)^2 + \Pr\left(\frac{\partial g}{\partial h}\right)^2$$

Table 2 Numerical values of thermophysical characteristics of base fluid and nanoparticles [7,20].

	$\sigma(\Omega.m)^{-1}$	$ ho \left(\mathit{kgm}^{-3} \right)$	k(W/KgK)	$c_p(W/mK)$
Ethylene glycol (EG)	1.06×10^{-6}	1114	0.252	2415
TiO_2	2.38×10^6	4250	8.9538	686.2

$$\begin{pmatrix}
\frac{\partial f(h,\bar{\xi})}{\partial h} \\
f(h,\bar{\xi}) \\
g(h,\bar{\xi})
\end{pmatrix}_{h=0} = \begin{pmatrix} 1 \\ 0 \\ 1 \end{pmatrix},$$
(26)

$$\begin{pmatrix} \frac{\partial f(h \to \infty, \overline{\xi})}{\partial h} \\ g(h \to \infty, \overline{\xi}) \end{pmatrix} = \begin{pmatrix} 0 \\ 0 \end{pmatrix}. \tag{27}$$

To obtain the two-equation model, we will introduce the two variables as given below

$$f^* = \frac{\partial f}{\partial \overline{\xi}} \text{ and } g^* = \frac{\partial g}{\partial \overline{\xi}}.$$
 (28)

Utilizing (23) in (14)-(17), we get

$$\left(\frac{\Delta_1}{\Delta_2}\right)\frac{\partial^3 f}{\partial h^3} + f\frac{\partial^2 f}{\partial h^2} - \left(\frac{\partial f}{\partial h}\right)^2 - \left(\frac{\Delta_3}{\Delta_2}\right)H_m^2\frac{\partial f}{\partial h} = \xi\left(\frac{\partial f}{\partial h}\frac{\partial f^*}{\partial h} - \frac{\partial^2 f}{\partial h^2}f^*\right),$$
(29)

$$\frac{\left(\frac{\Delta_{4}}{\Delta_{5}}\right)\frac{\partial^{2}g}{\partial h^{2}} + \left(\frac{\Delta_{1}}{\Delta_{5}}\right)\Pr\bar{\xi}^{2}\left(\frac{\partial^{2}f}{\partial h^{2}}\right)^{2} + \left(\frac{\Delta_{3}}{\Delta_{5}}\right)\Pr H_{m}^{2}\bar{\xi}^{2}\left(\frac{\partial f}{\partial h}\right)^{2} + \Pr f\frac{\partial g}{\partial h} = \begin{cases} \\ \bar{\xi}\Pr\left(g^{*}\frac{\partial f}{\partial h} - \frac{\partial g}{\partial h}f^{*}\right) \end{cases}, \tag{30}$$

$$\begin{pmatrix}
\frac{\partial f(h,\overline{\xi})}{\partial h} \\
f(h,\overline{\xi}) + \overline{\xi}f^*(h,\overline{\xi}) \\
g(h,\overline{\xi})
\end{pmatrix}_{h=0} = \begin{pmatrix} 1 \\ 0 \\ 1 \end{pmatrix},$$
(31)

$$\begin{pmatrix}
\frac{\partial f(h \to \infty, \overline{\xi})}{\partial h} \\
g(h \to \infty, \overline{\xi})
\end{pmatrix} = \begin{pmatrix} 0 \\
0 \end{pmatrix}.$$
(32)

Because of the introduction of two more independent variables, namely f^* and g^* , we need two more equations (called subsidiary equations) to solve system (24)–(27). To accomplish this, we differentiated system (24)–(27) with respect to the $\bar{\xi}$ and ignoring the terms containing the derivative of f^* and g^* with respect to $\bar{\xi}$, we get

$$\left(\frac{\Delta_{1}}{\Delta_{2}}\right)\frac{\partial^{3} f^{*}}{\partial h^{3}} + f\frac{\partial^{2} f^{*}}{\partial h^{2}} + 2f^{*}\frac{\partial^{2} f}{\partial h^{2}} - 3\frac{\partial f}{\partial \eta}\frac{\partial f^{*}}{\partial \eta} - \left(\frac{\Delta_{3}}{\Delta_{2}}\right)H_{m}^{2}\frac{\partial f^{*}}{\partial h} = \xi\left(\left(\frac{\partial f^{*}}{\partial h}\right)^{2} - f^{*}\frac{\partial^{2} f^{*}}{\partial h^{2}}\right),\tag{33}$$

$$\left(\frac{\Delta_{4}}{\Delta_{5}}\right)\frac{\partial^{2}g^{*}}{\partial h^{2}} + 2\left(\frac{\Delta_{1}}{\Delta_{5}}\right)\Pr\bar{\xi}\left(\frac{\partial^{2}f}{\partial h^{2}}\right)^{2} + 2\left(\frac{\Delta_{1}}{\Delta_{5}}\right)\Pr\bar{\xi}^{2}\left(\frac{\partial^{2}f}{\partial h^{2}}\right)\left(\frac{\partial^{2}f^{*}}{\partial h^{2}}\right) + 2\Pr H_{m}^{2}\left(\frac{\Delta_{3}}{\Delta_{5}}\right)\left(\xi\left(\frac{\partial f}{\partial h}\right)^{2} + \overline{\xi}^{2}\frac{\partial f}{\partial h}\frac{\partial f^{*}}{\partial h}\right) \\
+ \Pr\left(f\frac{\partial g^{*}}{\partial h} + 2f^{*}\frac{\partial g}{\partial h}\right) = \Pr\left(g^{*}\frac{\partial f}{\partial h} + \overline{\xi}g^{*}\frac{\partial f^{*}}{\partial h} - \overline{\xi}f^{*}\frac{\partial g^{*}}{\partial h}\right)\right\}, \tag{34}$$

$$\begin{pmatrix}
\frac{\partial f^*(h,\overline{\xi})}{\partial h} \\
f^*(h,\overline{\xi}) \\
g^*(h,\overline{\xi})
\end{pmatrix} = \begin{pmatrix} 0 \\ 0 \\ 0 \end{pmatrix},$$
(35)

$$\begin{pmatrix}
\frac{\partial f^*(h \to \infty, \overline{\xi})}{\partial h} \\
g^*(h \to \infty, \overline{\xi})
\end{pmatrix} = \begin{pmatrix} 0 \\ 0 \end{pmatrix}.$$
(36)

Equations (24)–(27) and (33)-(36) are referred to as the two-equation model and are solved using a generalized differential quadrature method. The key steps of the implemented numerical scheme are illustrated in the flowchart shown in Fig. 2.

5. Second law analysis (entropy generation minimization)

For the current problem, we can compute the rate of entropy generation as follows:

$$E_{G} = \frac{k_{nf}}{T^{*2}} \left(\frac{\partial T^{*}}{\partial y}\right)^{2} + \frac{\mu_{nf}}{T^{*}} \left(\frac{\partial U^{*}}{\partial y}\right)^{2} + \frac{\sigma_{nf} H_{0}^{2} U^{*2}}{T^{*}}.$$
(37)

Utilizing (13) in (32) we get

$$E_{N} = \frac{E_{G}}{E_{G0}} = \frac{\Delta_{4}}{(g + \Theta)^{2}} \left(\frac{\partial g}{\partial h}\right)^{2} + Ec.Pr \frac{\Delta_{1}}{g + \Theta} \left(\frac{\partial^{2} f}{\partial h^{2}}\right)^{2} + Ec.Pr.H_{m}^{2} \frac{\Delta_{3}}{g + \Theta} \left(\frac{\partial f}{\partial h}\right)^{2}.$$
(38)

Here, E_N shows dimensionless entropy generation, E_{G0} indicates characteristic entropy and Θ represents the temperature difference parameter and is given by

$$\left. \begin{array}{l} E_{G0} = \frac{s_0 k_{bf}}{\nu_{bf}} \\ \Theta = \frac{T_A^*}{T_s^* - T_A^* A} = \frac{T_A^*}{\Delta T^*} \end{array} \right\}.$$
(39)

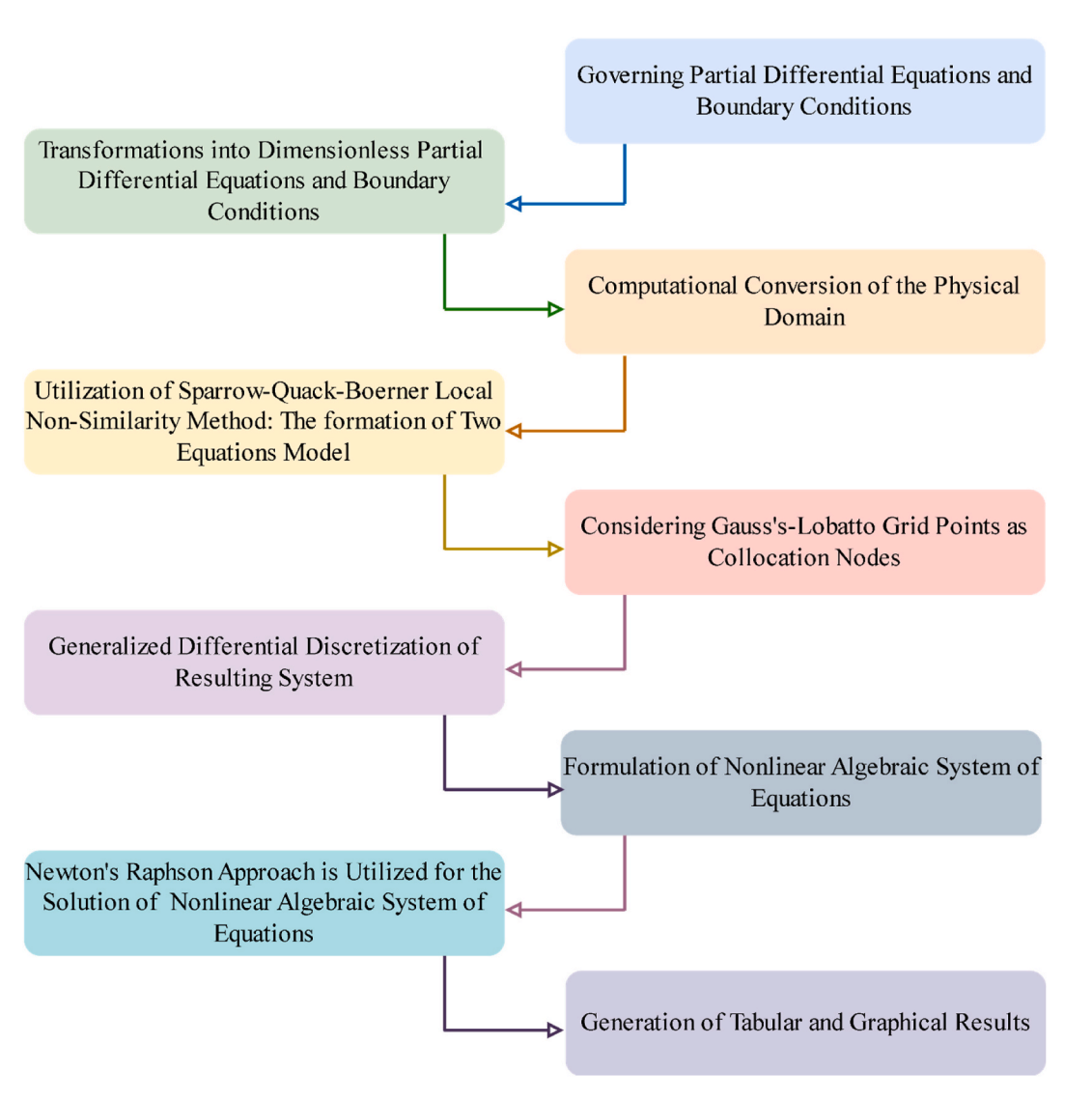


Fig. 2. Flowchart depicting the key steps of generalized differential quadrature scheme.

The important irreversibility number, called the Bejan number, is given by

$$B_{N} = \frac{\frac{k_{nf}}{T^{*2}} \left(\frac{\partial T^{*}}{\partial y}\right)^{2}}{\frac{k_{nf}}{T^{*2}} \left(\frac{\partial T^{*}}{\partial y}\right)^{2} + \frac{\mu_{nf}}{T^{*}} \left(\frac{\partial U^{*}}{\partial y}\right)^{2} + \frac{\sigma_{nf}H_{0}^{2}U^{*2}}{T^{*}}}.$$

$$(40)$$

Utilizing (13) in (40) we get

$$B_{N} = \frac{\Delta_{4} \left(\frac{\partial g}{\partial h}\right)^{2}}{\Delta_{4} \left(\frac{\partial g}{\partial h}\right)^{2} + \Delta_{1} \left(\frac{\partial^{2} f}{\partial h^{2}}\right)^{2} (g + \Theta) E c. P r + \Delta_{3} (g + \Theta) \left(\frac{\partial f}{\partial h}\right)^{2} E c. P r. H_{m}^{2}}$$

$$(41)$$

The objective of this section is to examine how effective physical flow parameters affect nanofluid velocity f'(h), temperature g(h),

6. Results and discussion

entropy generation number $E_N(h)$, and Bejan number profiles $B_N(h)$. Throughout the graphical representation, the dimensionless parameters $\bar{\xi}, \phi, H_m, \Theta$ and Pr have default values 0.1, 0.02, 0.3, 1.0 and 150.4583 respectively. To examine graphically the impacts of flow parameters on quantities of interest, the defined range of the flow parameters are $\{\bar{\xi}=0.1,0.15,0.25,0.35\}, \{\phi=0.01,0.02,0.03,0.03,0.03\}$ 0.035}, $\{H_m = 0.1, 0.3, 0.5, 0.7\}$ and $\{\Theta = 1.0, 2.0, 3.0, 4.0\}$. Validation of numerical results in a viscous fluid (viscous fluid, excluding nanofluid and ethylene glycol) were performed using previously published data (see Table 3). Most importantly, we have found a high degree of agreement between the present results and those of the literature, demonstrating the accuracy and validity of our numerical simulation. Table 4 presents the Nusselt number $\left(\frac{Nu_x}{\sqrt{Re_x}} = -(\Delta_4)\frac{\partial g(0,\bar{\xi})}{\partial h}\right)$ variations with change in physical flow parameters. An observation reveals that the Nusselt number decreases as the magnitude of H_m and ϕ increase in both cases, with and without aggregation. In comparison, the rate of reduction is notably swifter in the scenario involving nanoparticle aggregation, as opposed to the case without aggregation. Physically, when the Hartmann number rises, which denotes a strong magnetic field, convective heat transmission within the fluid can be suppressed. The reason for this suppression is that the fluid motion is restrained by the magnetic field, which lowers the velocity gradients. As a result, the convective heat transfer rate drops, which lowers the Nusselt number. Further, a decrement in Nusselt number with ϕ can be explain as, the overall viscosity of a fluid increase when nanoparticles are present. Increased viscosity causes reduced fluid mobility and increased internal flow resistance. A decrease in the Nusselt number might result from this increase in viscosity, which can obstruct convective heat transmission. Table 5 outlines the quantitative values of heat transfer augmentation in relation to the ascending values of ϕ . It is found that the heat transfer enhancement increases with ϕ and is high in the presence of NPs aggregation. Physically, Nanoparticles frequently exhibit thermal conductivities that are notably greater than those of the working fluid. The adding of nanoparticles results in an enhancement of the effective thermal conductivity of the mixture. A greater thermal conductivity facilitates the more effective conduction of heat inside the fluid, hence improving the process of heat transfer. Additionally, the heat transfer rate is high in the case of NPs aggregation because aggregation can create conductive paths within the nanofluid, enhancing its effective thermal conductivity. This can lead to improved heat transfer rates. We plot graphs (Figs. 3-14) for two cases, namely, with and without nanoparticle aggregation. The impact of the local non-similarity variable, which corresponds to the Eckert number, on the temperature profile g(h) is illustrated in Fig. 3. This depiction encompasses two distinct scenarios: one where nanoparticles (NPs) aggregation is not involved and the other where it is considered. It has been observed that a rise in $\bar{\xi}$ values will cause a rise in temperature distribution. From a physical perspective, an increase in $\bar{\xi}$ will increase the frictional forces among the fluid layers. Consequently, kinetic energy undergoes conversion into thermal energy, leading to an observable rise in the temperature profile. The effect of $\bar{\xi}$ on entropy generating in TiO_2/EG nanofluid with and without NPs aggregation is shown in Fig. 4. Entropy generation $E_N(h)$ shows increasing behaviour with rising values of the local non-similarity variable. This is because

Table 3Validation of the numerical results has been performed using existing data for a viscous fluid, excluding the effects of nanofluids and ethylene glycol.

H_m	ξ	Pr	Results of [62] (Bvp5c)	Present Results (GDQM)
0.0	0.5	3.0	0.9940803	0.9940803
0.5	0.5	3.0	0.8915465	0.8915467
1.0	0.5	3.0	0.6219926	0.6219925
1.5	0.5	3.0	0.2517937	0.2517932
1.0	0.1	3.0	1.0570826	1.0570821
1.0	0.2	3.0	1.0026963	1.0026963
1.0	0.3	3.0	0.9120527	0.9120529
1.0	0.4	3.0	0.7851512	0.7851510
1.0	0.5	0.7	0.2337296	0.2337296
1.0	0.5	1.2	0.3466271	0.3466270
1.0	0.5	2.7	0.5842767	0.5842769
1.0	0.5	3.0	0.6219926	0.6219923

Table 4Variation of Nusselts number with physical flow parameters.

H_m	ξ	φ	$rac{Nu_x}{\sqrt{\mathrm{Re}_x}} = -\left(\Delta_4\right) rac{\partial g(0, \overline{\xi})}{\partial h}.$ With Aggregation	$rac{Nu_x}{\sqrt{\mathrm{Re}_x}} = -\left(\Delta_4\right) rac{\partial \mathrm{g}(0,\overline{\xi})}{\partial h}.$ Without Aggregation
0.0			9.411402844	9.302261823
0.5	0.5	0.035	8.583762938	8.698735124
1.0	0.0	0.000	5.630763025	6.573820046
S_{LP}			-3.780	-2.728
- Li	0.1		10.19557530	9.914145218
0.7	0.2	0.035	9.883223642	9.682118178
	0.3		9.362637541	9.295406444
S_{LP}			-4.164	-3.093
		0.01	7.877799443	7.980836021
0.7	0.5	0.02	7.804861089	8.013245173
		0.03	7.731654112	8.043559354
S_{LP}			-7.307	3.136

Table 5 Numerical quantifications pertaining to the augmentation of heat transfer H_{TE} with and without nanoparticles aggregation at different values of ϕ and by taking $H_m = 0.7$ and $\xi = 0.5$.

$H_{TE} = \left \frac{Nu_x \text{Re}_x^{-1/2}(nanofluid) - Nu_x \text{Re}_x^{-1/2}(base fluid)}{Nu_x \text{Re}_x^{-1/2}(base fluid)} \right \times 100.\%$		
φ	With Aggregation	Without Aggregation
0.5 %	0.421 %	0.220 %
1.0 %	0.862 %	0.434 %
1.5 %	1.317 %	0.641 %
2.0 %	1.780 %	0.842 %
2.5 %	2.244 %	1.036 %
3.0 %	2.701 %	1.223 %
3.5 %	3.140 %	1.404 %

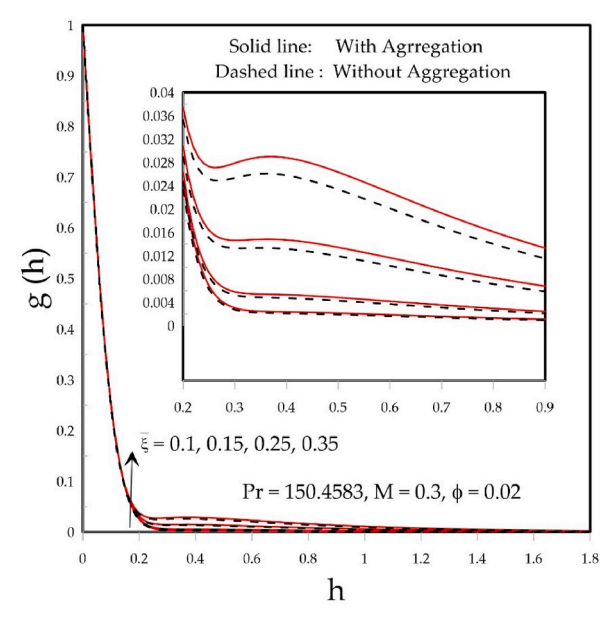


Fig. 3. The impact of $\overline{\xi}$ on g(h).

viscous dissipation is an irreversible process and leads to enhanced entropy generation. Furthermore, NPs aggregation leads to higher entropy generation as compared to the without NPs aggregation. Physically speaking, when clusters form as a result of nanoparticle aggregation, the viscosity of the nanofluid may rise. Increased entropy generation may result from this, as it may cause higher levels of viscous dissipation inside the boundary layer flow. Bejan number $B_N(h)$ profile for the different local non-similarity variable is shown

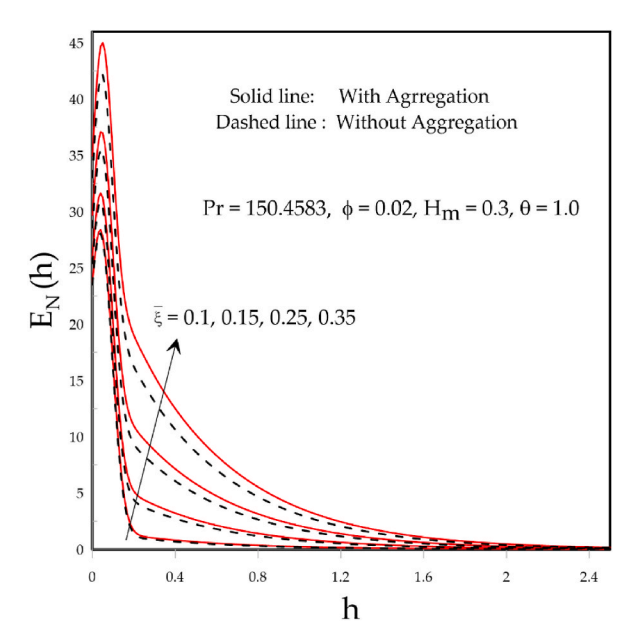


Fig. 4. The impact of $\overline{\xi}$ on $E_N(h)$.

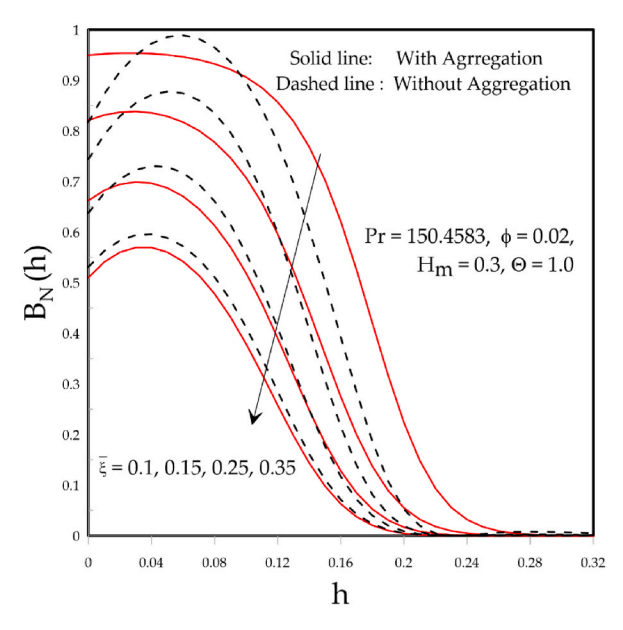


Fig. 5. The impact of $\overline{\xi}$ on $B_N(h)$.

in Fig. 5. As shown in Fig. 5, there is a decreasing trend in the Bejan number with an increase in the parameter $\bar{\xi}$.

Fig. 6 illustrates the temperature profile for various volume fractions ϕ of nanoparticles. By adding more TiO_2 nanoparticles, the nanofluid becomes more thermally conductive. As a result, the operational nanofluid is more conductive and raises the temperature profile of the TiO_2/EG nanofluid. Fig. 7 illustrates how ϕ influences entropy generation in both cases. An increase in the values of ϕ amplifies entropy generation in both scenarios. This occurs because the existence of nanoparticles adds extra frictional resistance to the fluid flow. Greater viscosity leads to an amplified dissipation of energy inside the flow, resulting in an elevated generation of entropy. Additionally, the rate of entropy generation is low in the absence of nanoparticle (NPs) aggregation. In Fig. 8, the results illustrate that the irreversibility caused by heat transfer at the surface of the stretching sheet is higher in nanofluid with NPs aggregation as compared to the nanofluid without NPS aggregation. Furthermore, beyond a specific distance from the solid boundary, the Bejan number decreases as the values of ϕ increase.

A decrement in the velocity profile f'(h) is noticed with increasing the magnetic parameter H_m as shown in Fig. 9. From a physical

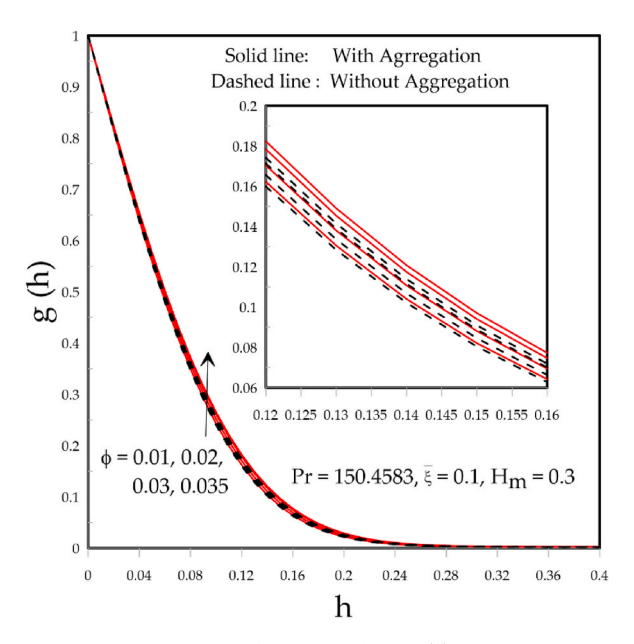


Fig. 6. The impact of ϕ on g(h).

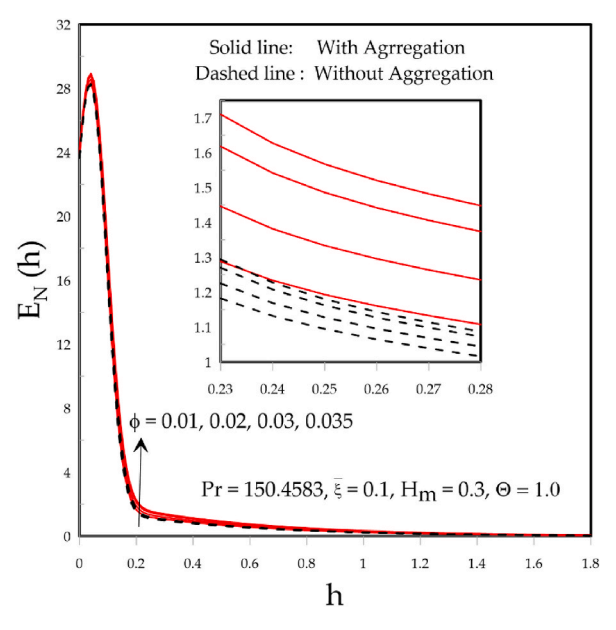


Fig. 7. The impact of ϕ on $E_N(h)$.

perspective, an increase in H_m implies a stronger magnetic field. In turn, the Lorentz force increases and decelerates the TiO_2/EG nanofluid. Boosts in the temperature profile are noticed with increasing the magnitude of the applied magnetic field as shown in Fig. 10. The reason for this outcome is the enhancement of Joule heating with increasing H_m . Additionally, the temperature of the nanofluid TiO_2/EG is higher in presence of nanoparticle (NPs) aggregation. This can be attributed to the superior effective thermal conductivity associated with NPs aggregation. Due to the resistance provided by the magnetic field and Joule heating, the entropy production boosts with growing values of H_m as presented in Fig. 11. As demonstrated in Fig. 12, a decrease in the Bejan number is seen in conjunction with an increase in the magnetic parameter.

Fig. 13 demonstrates the influence of temperature differences parameter Θ on entropy generation. For both cases, with and without NPs aggregation, the decline in the profile of $E_N(h)$ is observed with the rise in Θ . The magnitude of Θ escalates as the operating temperature differential, ΔT^* , diminishes (refer to Eq. (39)), consequently resulting in a reduction in the heat transfer rate. This reduction in the heat transfer rate yields a corresponding decline in the quantity of entropy generated within the boundary layer region. Alternatively, achieving the main goal of second law analysis, which is to minimize entropy generation (EG), can be

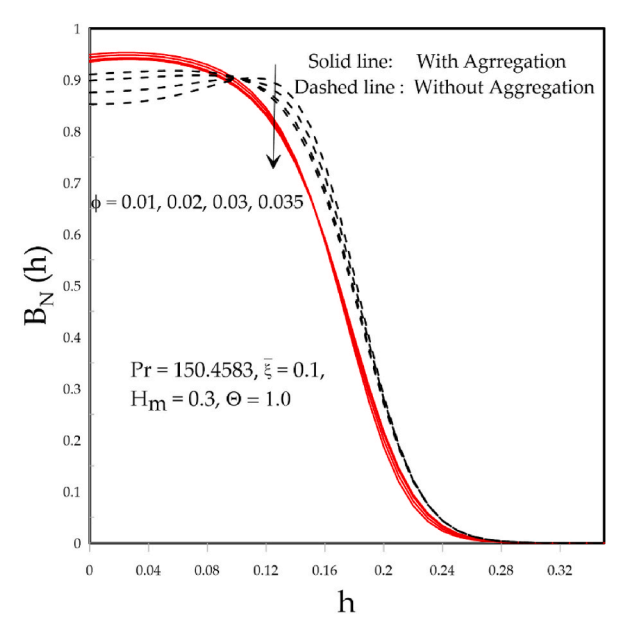


Fig. 8. The impact of ϕ on $B_N(h)$.

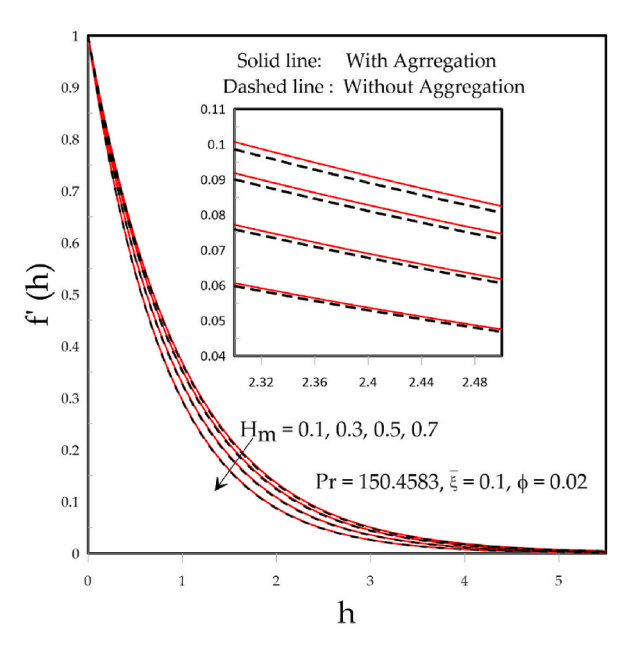


Fig. 9. The impact of H_m on f'(h).

accomplished by reducing the operating temperature ΔT^* . Fig. 14 displays the profile of the Bejan number for several values of Θ . Escalating values of Θ indicate a reduction in temperature difference between the stretched surface and ambient fluid. As a result, thermal irreversibility reduces, as presented in Fig. 14.

7. Concluding remarks

An examination of heat transfer and entropy generation in the local dissipative flow of nanofluid is conducted, considering the impact of nanoparticle aggregation. The Maxwell-Bruggeman and Kreiger-Dougherty models are used to represent the thermal conductivity and effective viscosity of a nanofluid containing aggregated nanoparticles, respectively. The following are potential conclusions drawn from this investigation.

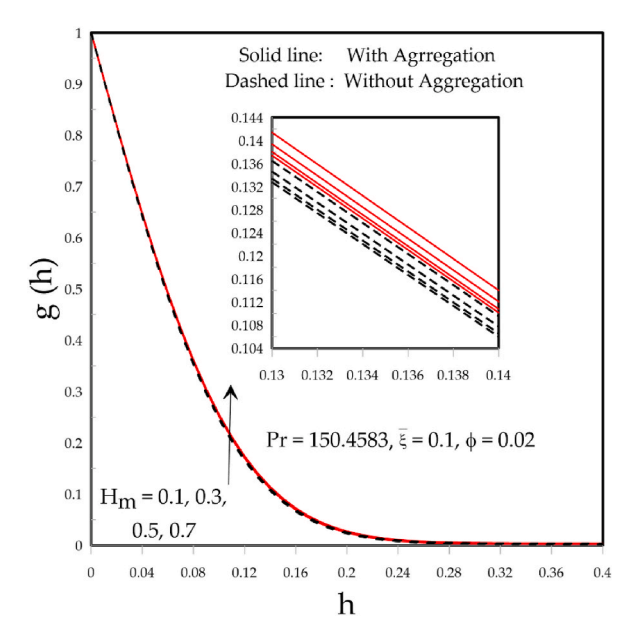


Fig. 10. The impact of H_m on g(h).

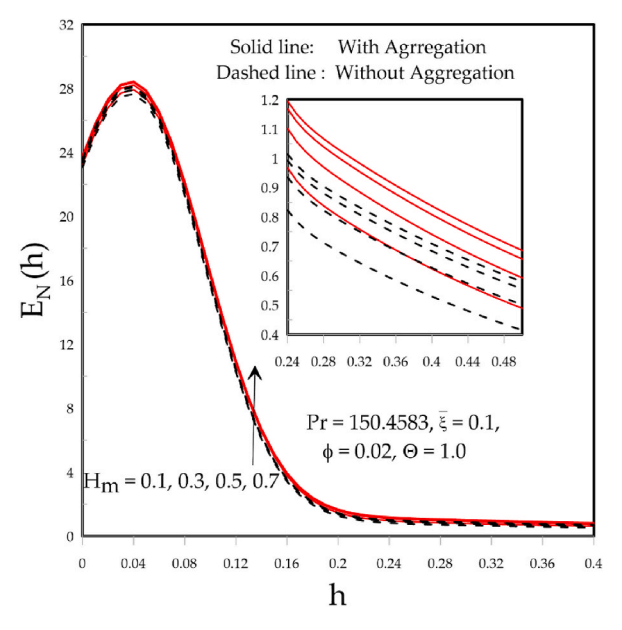


Fig. 11. The impact of H_m on $E_N(h)$.

- Thermal boundary layers over linearly stretched surfaces do not permit similarity transformations in the presence of viscous dissipation and constant wall temperatures.
- Local non-similarity is caused by viscous dissipation when the temperature remains constant at the solid boundary.
- The rate of heat transfer augmentation increases with the volume fraction of nanoparticles in both situations (with and withzout aggregation).
- Aggregation increases the rate of heat transmission at a rapid rate.

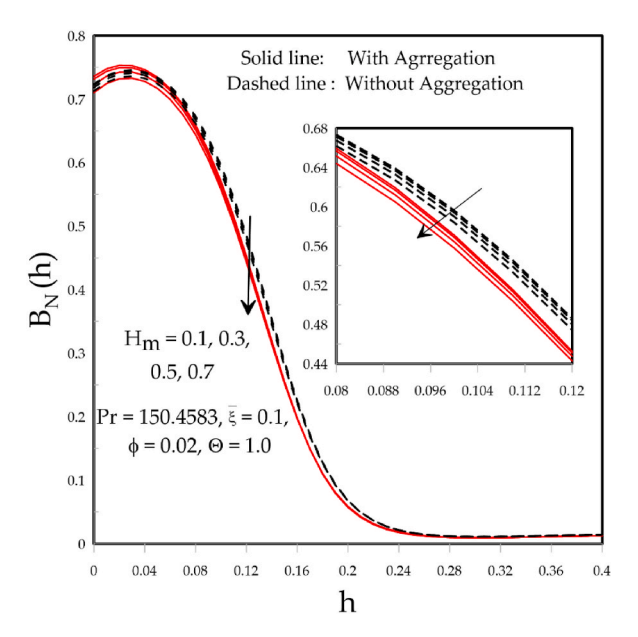


Fig. 12. The impact of H_m on $B_N(h)$.

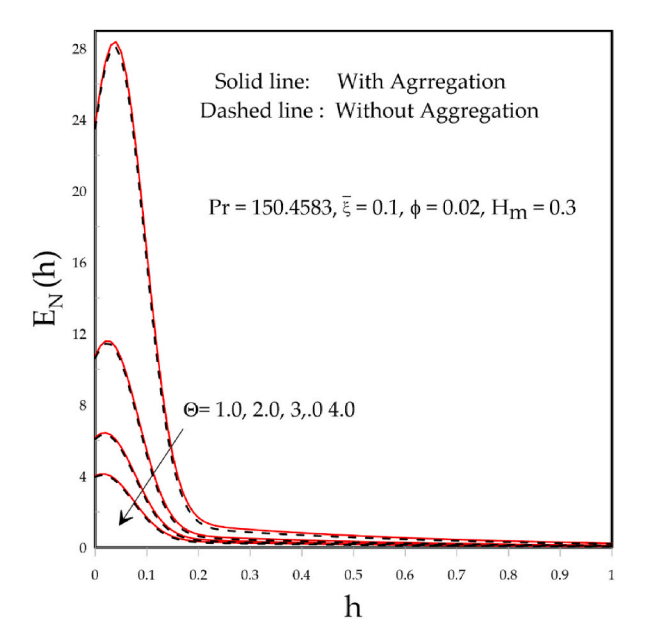


Fig. 13. The impact of Θ on $E_N(h)$.

- Nusselt's number decreases more rapidly with aggregation compared to without aggregation, with increasing values of the Hartman number and the streamwise transformed coordinate.
- Nanofluid velocity decelerated with increasing the Hartman number.
- The velocity profile without aggregation is lower than the velocity profile with aggregation.
- Temperature and entropy are found to be increasing functions of streamwise transformed coordinate, Hartman number, and nanoparticles volume fraction
- High entropy generation and thermal profile are found with NPs aggregation.
- Bejan's number profile declined with growing streamwise transformed coordinate Hartman number and temperature difference parameter values.
- The decrement in entropy generation and Bejan number is observed with growing values of the temperature difference parameter.
- In the future, studying the second law analysis of time-dependent, two-dimensional, local, non-similar flow in conjunction with nanoparticle aggregation will be quite interesting. The numerous industrial and engineering applications of nanofluids, including

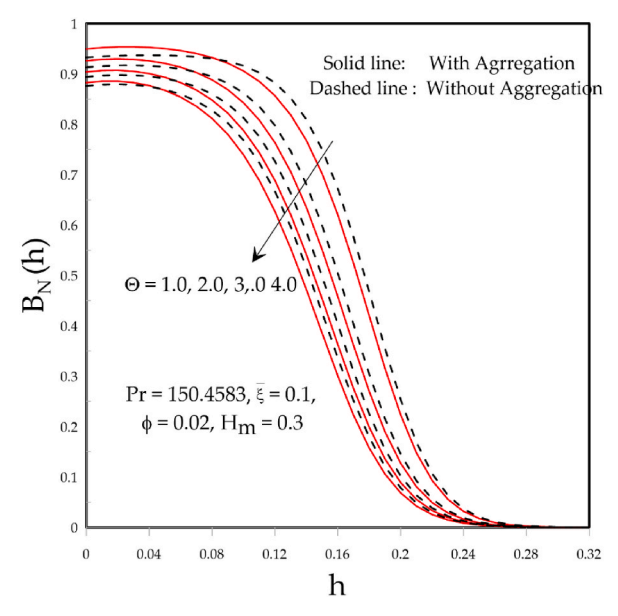


Fig. 14. The impact of Θ on $E_N(h)$.

cancer treatment, implantable nanotherapeutic devices, microelectromechanical systems, and cooling processes, make this work significant.

CRediT authorship contribution statement

Muhammad Idrees Afridi: Writing – review & editing, Writing – original draft, Software, Investigation, Conceptualization, Funding acquisition. **Abdullah Alhushaybari:** Validation, Visualization, Writing – original draft, Writing – review & editing, Methodology, Software. **Ali J. Chamkha:** Writing – review & editing, Writing – original draft, Supervision, Software.

Funding

This research was funded by Taif University, Saudi Arabia, project No. (TU-DSPP-2024-145).

Declaration of competing interest

The author declare that he have no known competing financial interests or personal relationships that could have appeared to influence the work reported in this paper.

Acknowledgement

The authors extend their appreciation to Taif University, Saudi Arabia, for supporting this work through project number (TU-DSPP-2024-145).

Data availability

No data was used for the research described in the article.

References

- [1] S.U.S. Choi, Enhancing thermal conductivity of fluids with nanoparticles, The Proceedings of the 1995 ASME International Mechanical Engineering Congress and Exposition 66 (1995) 99–105. San Francisco, USA, ASME, FED 231/MD.
- [2] W. J. Minkowycz, E M Sparrow and J. P. Abraham, Nanoparticle Heat Transfer and Fluid Flow, CRC Press,
- [3] M. Hatami and D. Jing, Nanofluids: Mathematical, Numerical, and Experimental Analysis, Academic Press.
- [4] K.R.V. Subramanian, T. N. Rao and A. Balakrishnan, Nanofluids and their Engineering Applications, CRC Press.
- [5] B. Bhanvase and D. Barai, Nanofluids for Heat and Mass Transfer: Fundamentals, Sustainable Manufacturing and Applications, Academic Press.
- [6] M. Turkyilmazoglu, Free and circular jets cooled by single phase nanofluids, Eur. J. Mech. B Fluid 76 (2019) 1-6.
- [7] K. A. M Alharbi Adnan, M.Z. Bani-Fwaz, S.M. Eldin, M.F. Yasse, Numerical heat performance of TiO2/Glycerin under nanoparticles aggregation and nonlinear radiative heat flux in dilating/squeezing channel, Case Stud. Therm. Eng. 41 (2023) 102568.

- [8] Sameh E. Ahmed, A.A.M. Arafa, Sameh A. Hussein, Cattaneo-christov double-diffusion and hydrothermal flow of sutterby tri, hybrid and mono-nanofluids with oxytactic microorganism, Int. J. Ambient Energy 44 (2023) 2200–2213.
- [9] Sameh E. Ahmed, Anas A.M. Arafa, Sameh A. Hussein, Zeinab Morsy, Time-dependent squeezing flow of variable properties ternary nanofluids between rotating parallel plates with variable magnetic and electric fields, Numer. Heat Tran., Part A: Applications (2023) 1–30.
- [10] Adnan, W. Abbas, N.M. Said, N.K. Mishra, Z. Mahmood, M. Bilal, Significance of coupled effects of resistive heating and perpendicular magnetic field on heat transfer process of mixed convective flow of ternary nanofluid, J. Therm. Anal. Calorim. 149 (2024) 879–892.
- [11] Sanatan Das, Akram Ali and Rabindra Nath Jana, Numerically framing the impact of magnetic field on nanofluid flow over a curved stretching surface with convective heating, World Journal of Engineering, Vol. 18 No. 6, pp. 938-947. https://doi.org/10.1108/WJE-11-2020-0587.
- [12] S. Sarkar, R.N. Jana and S. Das, Activation energy impact on radiated magneto-Sisko nanofluid flow over a stretching and slipping cylinder: entropy analysis, Multidiscip. Model. Mater. Struct., Vol. 16 No. 5, pp. 1085-1115. https://doi.org/10.1108/MMMS-09-2019-0165.
- [13] Jitendra Kumar Singh, Gauri Shanker Seth, Syed M. Hussain, Thermal performance of hydromagnetic nanofluid flow within an asymmetric channel with arbitrarily conductive walls filled with darcy-brinkman porous medium, J. Magn. Magn Mater. 582 (2023) 171034.
- [14] Syed M. Hussain, Mariam Imtiaz, Kalsoom Bibi, Sadique Rehman, Wasim Jamshed, Mohamed R. Eid, Sayed M. El Din, Error analysis of zirconium and zinc oxides/kerosene oil-based hybrid nanofluid flow between rotating disks: an innovative case study, Case Stud. Therm. Eng. (51) (2023) 103549.
- [15] Modassir Hussain Syed, Umair Khan, Aurang Zaib, Anuar Ishak, Ioannis E. Sarris, Numerical computation of mixed convective entropy optimized in darcy-forchheimer flow of cross nanofluids through a vertical flat plate with irregular heat source/sink, Tribol. Int. (187) (2023) 108757.
- [16] Shahanaz Parvin, Siti Suzilliana Putri Mohamed Isa, Fuad S. Al- Duais, Syed M. Hussain, Wasim Jamshed, Rabia Safdar and Mohamed R. Eid, The flow, thermal and mass properties of Soret-Dufour model of magnetized Maxwell nanofluid flow over a shrinkage inclined surface, PLoS One 17(4): e0267148. https://doi.org/10.1371/journal.pone.0267148.
- [17] D. Mohanty, G. Mahanta, S. Shaw, M. Das, Thermosolutal Marangoni stagnation point GO–MoS2/water hybrid nanofluid over a stretching sheet with the inclined magnetic field, Int. J. Mod. Phys. B (38) (2024) 2450024.
- [18] S.S. Samantaray, A. Misra, S. Shaw, J. Prakash, V.S. Pandey, M.K. Nayak, Investigating to chemically reactive and radiative Darcy/non-Darcy stagnation point flow of ternary composite nanofluids with moderate Prandtl numbers. Int. J. Model. Simulat. (2023). https://doi.org/10.1080/02286203.2023.2188515.
- [19] Debashis Mohanty, Ganeswar Mahanta, Sachin Shaw, Analysis of irreversibility for 3-D MHD convective Darcy–Forchheimer Casson hybrid nanofluid flow due to a rotating disk with Cattaneo–Christov heat flux, Joule heating, and nonlinear thermal radiation, Numer. Heat Tran., Part B: Fundamentals 84 (2) (2023) 115–142, https://doi.org/10.1080/10407790.2023.2189644.
- [20] H. Chen, Y. Ding, Y. He, C. Tan, Rheological behaviour of ethylene glycol based titania nanofluids, Chem. Phys. Lett. 444 (2007) 333–337, https://doi.org/10.1016/j.cplett.2007.07.046.
- [21] J. Chen, C.Y. Zhao, B.X. Wang, Effect of nanoparticle aggregation on the thermal radiation properties of nanofluids: an experimental and theoretical study, Int. J. Heat Mass Tran. 154 (2020) 11–14, https://doi.org/10.1016/j.ijheatmasstransfer.2020.119690.
- [22] M. Bagheri Motlagh, M. Kalteh, Molecular dynamics simulation of nanofluid convective heat transfer in a nanochannel: effect of nanoparticles shape, aggregation and wall roughness, J. Mol. Liq. 318 (2020) 114028, https://doi.org/10.1016/j.molliq.2020.114028. Nov.
- [23] K. Swain, B. Mahanthesh, Thermal enhancement of radiating magneto- nanoliquid with nanoparticles aggregation and Joule heating: a three-dimensional flow, Arabian J. Sci. Eng. 46 (6) (Jun. 2021) 5865–5873, https://doi.org/10.1007/s13369-020-04979-5.
- [24] A.S. Sabu, J. Mackolil, B. Mahanthesh, A. Mathew, Nanoparticle aggregation kinematics on the quadratic convective magnetohydrodynamic flow of nanomaterial past an inclined flat plate with sensitivity analysis, Proc. Inst. Mech. Eng. Part E J. Process Mech. Eng. (2021), https://doi.org/10.1177/ 09544089211056235
- [25] B. Mahanthesh, Flow and heat transport of nanomaterial with quadratic radiative heat flux and aggregation kinematics of nanoparticles, Int. Commun. Heat Mass Tran. 127 (Oct. 2021) 105521, https://doi.org/10.1016/j.icheatmasstransfer.2021.105521.
- [26] J. Mackolil, B. Mahanthesh, Inclined magnetic field and nanoparticle aggregation effects on thermal Marangoni convection in nanoliquid: a sensitivity analysis, Chin. J. Phys. 69 (Feb. 2021) 24–37, https://doi.org/10.1016/j.cjph.2020.11.006.
- [27] M. Turkyilmazoglu, Exact momentum layer and thermal field solutions for the fluid flow due to a moving/deforming Riga plate, Int. J. Therm. Sci. 208 (2025) 109448.
- [28] Sameh E. Ahmed, Anas A.M. Arafa, Sameh A. Hussein, Hydrothermal dissipative nanofluid flow over a stretching Riga plate with heat and mass transmission and shape effects, J. Therm. Anal. Calorim. 149 (2024) 4855–4872.
- [29] Adnan, W. Ashraf, Thermal efficiency in hybrid (Al2O3-CuO/H2O) and ternary hybrid nanofluids (Al2O3-CuO-Cu/H2O) by considering the novel effects of imposed magnetic field and convective heat condition, Waves Random Complex Media (2022) 1–16.
- [30] Adnan, Heat transfer inspection in [(ZnO-MWCNTs)/water-EG(50:50)]hnf with thermal radiation ray and convective condition over a Riga surface, Waves Random Complex Media (2022) 1–15.
- [31] M. Turkyilmazoglu, Evidence of stretching/moving sheet-triggered nonlinear similarity flows: atomization and electrospinning with/without air resistance, Int. J. Numer. Methods Heat Fluid Flow 34 (2024) 3598–3614.
- [32] W. Aich, Adnan, G. Sarfraz, N.M. Said, M. Bilal, A.F.A. Elhag, A.M. Hassan, Significance of radiated ternary nanofluid for thermal transport in stagnation point flow using thermal slip and dissipation function, Case Stud. Therm. Eng. 51 (2023) 103631.
- [33] Z.S. Hafed, Sameh A. Hussein, Abdulaziz Alenazi, Anas A.M. Arafa, Sameh E. Ahmed, Impacts of Arrhenius energy and viscous dissipation on variable properties of viscoelastic nanofluid flow with slip velocity, Int. J. Model. Simulat. (2023) 1–19.
- [34] L. Kolsi, Ahmed Mir Adnan, T. Muhammad, M. Bilal, Zubair Ahmad, Numerical simulation of heat and mass transfer through hybrid nanofluid flow consists of polymer/CNT matrix nanocomposites across parallel sheets, Alex. Eng. J. 108 (2024) 319–331.
- [35] M. Turkyilmazoglu, Flow and heat transfer in annuli owing to inner shrinking and outer stationary cylinder, Chin. J. Phys. 89 (2024) 1899–1907.
- [36] M. Mushtaq, S. Asghar, M.A. Hossain, Mixed convection flow of second grade fluid along a vertical stretching flat surface with variable surface temperature, Heat Mass Tran. 43 (2007) 1049–1061.
- [37] P. Vyas, N. Srivastava, On dissipative radiative MHD boundary layer flow in a porous medium over a non-isothermal stretching sheet, J. Appl. Fluid Mech. 5 (2012) 23–31.
- [38] M.I. Afridi, M. Qasim, I. Khan, S. Shafie, A.S. Alshomrani, Entropy generation in magnetohydrodynamic mixed convection flow over an inclined stretching sheet, Entropy 19 (2017) 1–10.
- [39] R. Cortell, Viscous flow and heat transfer over a nonlinearly stretching sheet, Appl. Math. Comput. 184 (2007) 864-873.
- [40] M.I. Afridi, M. Qasim, I. Khan, Entropy generation minimization in MHD boundary layer flow over a slendering stretching sheet in the presence of frictional and Joule heating, J. Kor. Phys. Soc. 73 (2018) 1303–1309.
- [41] A.M. Megahed, Williamson fluid flow due to a nonlinearly stretching sheet with viscous dissipation and thermal radiation, Journal of the Egyptian Mathematical Society 27 (2019) 1–12.
- [42] M.K. Partha, P.V.S.N. Murthy, G.P. Rajasekhar, Effect of viscous dissipation on the mixed convection heat transfer from an exponentially stretching surface, Heat Mass Tran. 41 (2005) 360–366.
- [43] M.I. Afridi, M. Qasim, O.D. Makinde, Second law analysis of boundary layer flow with variable fluid properties, J. Heat Tran. 39 (2017) 104505.
- [44] M. Qasim, N. Riaz, D.C. Lu, S. Shafie, Three-dimensional mixed convection flow with variable thermal conductivity and frictional heating, Commun. Theor. Phys. 72 (2020) 035003.
- [45] M.I. Afridi, M.U. Ashraf, M. Qasim, A. Wakif, Numerical simulation of entropy transport in the oscillating fluid flow with transpiration and internal fluid heating by GGDQM, Waves Random Complex Media (2022), https://doi.org/10.1080/17455030.2022.2067371.
- [46] A. Bejan, A study of entropy generation in fundamental convective heat transfer, ASME, J. Heat Tran. 101 (1979) 718-725.
- [47] S. Mandal, S. Shaw, O.D. Makinde, Entropy analysis of thermo-solutal stratification of nanofluid flow containing gyrotactic microorganisms over an inclined radiative stretching cylinder, Therm. Sci. Eng. Prog. (34) (2022) 101379.

- [48] R. Mahato, M. Das, S.S.S. Sen, S. Shaw, Entropy generation on unsteady stagnation-point Casson nanofluid flow past a stretching sheet in a porous medium under the influence of an inclined magnetic field with homogeneous and heterogeneous reactions, Heat Transfer 51 (2022) 5723–5747.
- [49] M.I. Afridi, M. Qasim, Comparative study and entropy generation analysis of Cu–H2O and Ag–H2O nanofluids flow over a slendering stretching surface, J. Nanoflu. (7) (2018) 783–790, 8.
- [50] A.J. Chamkha, M. Ismael, A. Kasaeipoor, T. Armaghani, Entropy generation and natural convection of CuO-water nanofluid in C-shaped cavity under magnetic field, Entropy 18 (2016), https://doi.org/10.3390/e18020050.
- [51] A.S. Butt, A. Ali, Entropy analysis of flow and heat transfer caused by a moving plate with thermal radiation, J. Mech. Sci. Technol. 28 (2014) 343-348.
- [52] M.M. Rashidi, N. Freidoonimehr, Analysis of entropy generation in MHD stagnation-point flow in porous media with heat transfer, Int. J. Comput. Methods Eng. Sci. Mech. 15 (2014) 345–355.
- [53] O.D. Makinde, Entropy for MHD boundary layer flow and heat transfer over a flat plate with a convective surface boundary condition, Int. J. Exergy 10 (2012) 142–154.
- [54] M.M. Rashidi, F. Mohammadi, S. Abbasbandy, M.S. Alhuthali, Entropy generation analysis for stagnation point flow in a porous medium over a permeable stretching surface, J. Appl. Fluid Mech. 8 (2015) 753–765.
- [55] S. Das, R.N. Jana, O.D. Makinde, Entropy generation in hydromagnetic and thermal boundary layer flow due to radial stretching sheet with Newtonian heating, J. Heat Mass Trans. Res. 2 (2015) 51–61.
- [56] A.K.A. Hakeem, M. Govindaraju, B. Ganga, M. Kayalvizhi, Second law analysis for radiative MHD slip flow of a nanofluid over a stretching sheet with non-uniform heat source effect, Sci. Iran. 23 (2016) 1524–1538.
- [57] A. Sahoo, R. Nandkeolyar, Entropy generation and dissipative heat transfer analysis of mixed convective hydromagnetic flow of a Casson nanofluid with thermal radiation and Hall current, Sci. Rep. 11 (2021) 3926, https://doi.org/10.1038/s41598-021-83124-0.
- [58] K.K. Al-Chlaihawi, H.H. Alaydamee, A.E. Faisal, K. Al-Farhany, M.A. Alomari, Newtonian and non-newtonian nanofluids with entropy generation in conjugate natural convection of hybrid nanofluid-porous enclosures: a review, Heat Transfer 51 (2022) 1725–1745, https://doi.org/10.1002/htj.22372.
- [59] R.B. Bird, W.E. Stewart, E.N. Lightfoot, D.J. Klingenberg, Introductory Transport Phenomena, Wiley, 2014.
- [60] H. Hassan H, N. Regnier, C. Pujos, G. Defaye, Effect of viscous dissipation on the temperature of the polymer during injection molding filling, Poly. Sci. Eng. 48 (2008) 1199–1206.
- [61] M.G. Reddy, P. Padma, B. Shankar, Effects of viscous dissipation and heat source on unsteady MHD flow over a stretching sheet, Ain Shams Eng. J. 6 (2015) 1195–1201
- [62] Muhammad Idrees Afridi, Zhi-Min Chen, Nadia Riaz, Muhammad Qasim, Heat transfer and flow analysis over a linearly stretching sheet with constant wall temperature: novel local non-similar solutions in the presence of viscous heating, Z. Angew. Math. Mech. 103 (2023) e202300003, https://doi.org/10.1002/zamm.202300003.